Wind and Structures, Vol. 5, No. 6 (2002) 515-526
DOI: http://dx.doi.org/10.12989/was.2002.5.6.515

Wind flow over sinusoidal hilly obstacles located in a uniform flow

Sang-Joon Lee†, Hee-Chang Lim‡ and Ki-Chul Park‡†

Pohang University of Science & Technology, San 31 Hyoja-Dong, 790-784, Pohang, Korea
(Received March 5, 2001, Accepted March 22, 2002)

Abstract. The wind flow over two-dimensional sinusoidal hilly obstacles with slope (the ratio of height to half width) of 0.5 has been investigated experimentally and numerically. Experiments for single and double sinusoidal hill models were carried out in a subsonic wind tunnel. The mean velocity profiles, turbulence statistics, and surface pressure distributions were measured at the Reynolds number based on the obstacle height(h=40 mm) of 2.6×10^4. The reattachment points behind the obstacles were determined using the oil-ink dot and tuft methods. The smoke-wire method was employed to visualize the flow structure qualitatively. The finite-volume-method and the SIMPLE-C algorithm with an orthogonal body-fitted grid were used for numerical simulation. Comparison of mean velocity profiles between the experiments and the numerical simulation shows a good agreement except for the separation region, however, the surface pressure data show almost similar distributions.

Key words: hilly obstacle; numerical simulation; single hill; double hill; turbulence model; flow visualization.

1. Introduction

The flow over a complex terrain has received considerable attention recently. Especially, the flow over wavy obstacles becomes an important research subject and has many engineering applications such as evaluation of environment impact by pollutant dispersion, positioning of wind mills and airports, etc. Air pollution due to rapid industrialization has also attracted increasing attention as a public environmental problem. The sources of air pollution are often located at hilly terrain in which the pollutant dispersion is strongly influenced by local flow condition. The complex flow structure such as flow separation, downwash flow, abrupt change of flow direction, and disconnection of streamlines can be caused by topographical boundary conditions. Therefore, it is prerequisite to understand the flow field over hilly obstacles for predicting the wind environments and environmental impacts accurately.

There are several previous studies on the flow over wavy obstacles. Jackson and Hunt (1975) investigated the turbulent flow over a gentle-sloped hill using a linear analytic theory. Recently, Taylor (1997) reported the effect of the turbulent boundary layer flow over several topographies. Pearse (1982), Bowen *et al*. (1977) and Siegel (1976) carried out wind tunnel experiments and gave useful data for understanding the wind flow over hilly terrains. Glekas *et al*. (1987), Bergeles (1985), and recently Kim *et al*. (1997) simulated numerically the flow over a two-dimensional topography using the RANS

† Professor, Department of Mechanical Engineering
‡ Graduate Student, School of Environmental Engineering
‡† Research Engineer, Hyundai Motor Company

(Reynolds-Averaged Navier-Stokes) equation with some turbulence modelings. However, there were limited investigations on the turbulent structure of shear layer separated from the hill crest.

Most previous studies have investigated the flow over a simple topography within a neutrally buoyant atmospheric boundary layer. However, the wind flow over a complex hilly terrain has received relatively little attention. For example, there are few studies on flow over multiple hills, especially on the effect of gap distance between multiple hills. In addition, the study on flow over hilly obstacles embedded in a uniform flow is essential to understand the underlying basic physics of flow structure. The main objective of this study is to investigate the flow structure of wind over sinusoidal hilly terrains submerged in a uniform flow experimentally and numerically. The flow structure over a double-hill was compared with that over a single hill.

2. Experimental apparatus and method

The present experiments were carried out in a closed-return type subsonic wind tunnel with a test section of 0.72 m wide, 0.6 m high, and 6 m long. The free stream velocity U_∞ was fixed at 10 m/s and the corresponding Reynolds number based on the height of mountain hill (h=40 mm) was $Re=2.6\times 10^4$. Free stream turbulence intensity in the test section was less than 0.08% at U_∞=10 m/s. Wind tunnel test section and experiment setup are shown in Fig. 1.

The hill models with smooth surface were made of fiber reinforced plastic material and resin. The model hills have the sinusoid shape of $y=h/2(1+\cos(\pi x/L_2))$, where h is the height and L_1 is the half-length at the upwind mid-height of the hill. The hill slope is defined as the average slope for the upstream top-half of the hill crest, i.e., $s=h/(2L_1)$. For the double-hills, the gap distance between adjacent hills was varied to be G/L_1=1, 2, 3, and 6, respectively. In order to embed the sinusoidal obstacle in a nearly uniform flow, the distance between the sharp leading edge of the flat plate and the first obstacle was reduced as short as possible. The boundary layer thickness measured at upstream location of the first obstacle was about δ/h=0.125~0.15. The sinusoidal hill and coordinate system used in this study are shown in Fig. 2.

The schematic diagram of the velocity and pressure measurement system is shown in Fig. 3. For surface pressure measurements, pressure taps were installed along the longitudinal center plane of the model with a 5 mm interval. The pressure taps were connected to the scannivalve system (48J9-1) and analog pressure signal from the scannivalve was digitized by a high precision A/D converter (DT2838). At each channel, the pressure data of 16384 samples were acquired at a 500 Hz sampling rate, after low-pass filtering at 200 Hz. In scanning each channel, about 10 seconds time delay was given for dynamic pressure recovery.

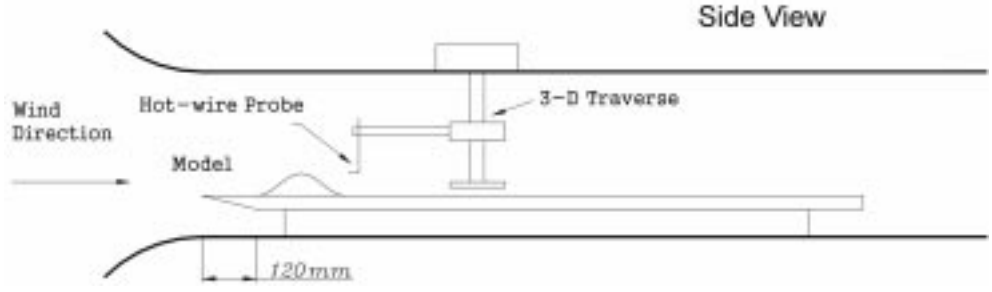

Fig. 1 Wind tunnel test section and experimental setup

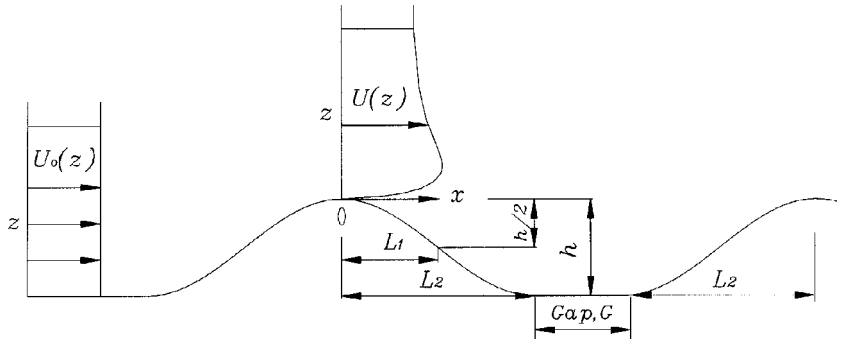

Fig. 2 Schematic diagram of the wind flow over sinusoidal hill models

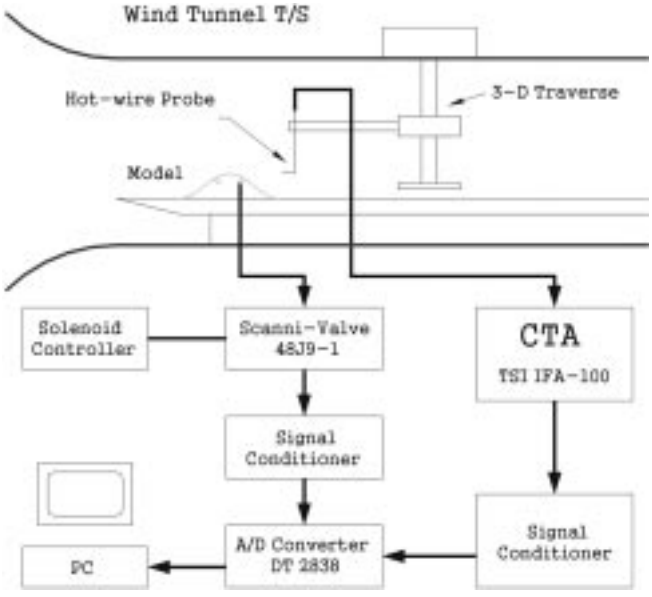

Fig. 3 Schematic diagram of the velocity and pressure measurement system

The pressure difference between the surface pressure p and the reference static pressure p_o was non-dimensionalized by the dynamic pressure with free-stream velocity U_∞ and air density δ to give the pressure coefficient C_p

$$C_p=(p-p_\infty)/0.5\rho U_\infty^2 \tag{1}$$

The pitot-static tube and hot-wire probe were traversed to measure spatial distributions of the mean velocity and turbulent intensity profiles. At each measurement point, velocity signals from the hot-wire probe were digitized at a 4 KHz sampling rate.

3. Numerical method

The numerical model used for the solution of the RANS (Reynolds-Averaged Navier-Stokes) equation was developed on the basis of the finite-volume method in an orthogonal, body-fitted coordinate system. The hybrid scheme (Patankar 1980) was used to approximate the convection terms and SIMPLE-C pressure correction algorithm was applied. The coordinate system employed in this study is the right-hand Cartesian coordinate system in which $x=0$ represents the location of the hill crest and the vertical coordinate z represents the height above terrain surface as shown in Fig. 2.

In the present numerical study, the standard $k-\varepsilon$ turbulence model and the low-Reynolds-number model were used. The standard $k-\varepsilon$ turbulence model has been used widely and validated in many engineering applications. It has achieved notable successes in a wide variety of practical applications, especially for several confined flows where the Reynolds stresses are most important. However, due to the underlying assumption of isotropic turbulent eddy-viscosity, the standard $k-\varepsilon$ turbulence model has some limitations in application to the flows with adverse pressure gradient. Therefore, the low-Reynolds-number model (Launder and Sharma 1974) has been employed in addition to the standard $k-\varepsilon$ turbulence model as an effective turbulence model, especially for separated shear flows. These models have been known to be simple, but reliable and efficient for this kind of flow analysis (Wilcox 1993).

The vectorized form of the governing equations in a Cartesian coordinate system is as follows :

$$E_x + F_z = S \tag{2}$$

and

$$E = \begin{pmatrix} \rho U \\ \rho UU - \mu_t U_x \\ \rho UW - \mu_t W_x \\ \rho Uk - \mu_t k_x/\sigma_k \\ \rho U\varepsilon - \mu_t \varepsilon_x/\sigma_\varepsilon \end{pmatrix} \quad F = \begin{pmatrix} \rho W \\ \rho WU - \mu_t U_z \\ \rho WW - \mu_t W_z \\ \rho Wk - \mu_t k_z/\sigma_k \\ \rho W\varepsilon - \mu_t \varepsilon_z/\sigma_\varepsilon \end{pmatrix} \quad S = \begin{pmatrix} 0 \\ (\mu_t U_x)_x + (\mu_t W_x)_z - p_x \\ (\mu_t U_z)_x + (\mu_t W_z)_z - p_z \\ G - \rho\varepsilon \\ (C_1 G - C_2 \rho\varepsilon)\varepsilon/k \end{pmatrix} \tag{3}$$

The subscripts x and z denote partial derivatives in the respective coordinate directions, and U and W are the x and z-component mean velocities. Physical quantities ρ, p, μ_t represent density, pressure, and turbulent viscosity coefficient, respectively.

The production rate G of turbulence kinetic energy in Eq. (3) is given as

$$G = \mu_t\{(U_z + W_x)^2 + 2(U_x^2 + W_z^2)\} \tag{4}$$

From the eddy viscosity hypothesis, the turbulent eddy viscosity is given by

$$\mu_t = \rho C_\mu k^2/\varepsilon \tag{5}$$

For the standard $k-\varepsilon$ turbulence model (Jones and Launder 1972), the following five empirical constants were used :

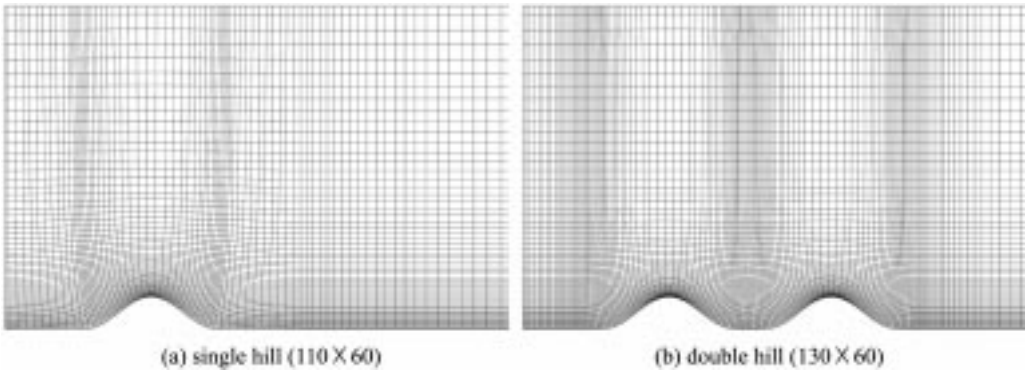

Fig. 4 Computational grids used in this study

$$C_\mu = 0.09, \quad C_1 = 1.44, \quad C_2 = 1.92$$
$$\sigma_k = 1.0, \quad \sigma_\varepsilon = \frac{\kappa^2}{(C_2 - C_1)\sqrt{C_\mu}} \tag{6}$$

where κ is von Karman constant ($\kappa = 0.41$)

The low-Reynolds-number model is a modified version of the standard $k-\varepsilon$ turbulence model for analyzing turbulent flows at low Reynolds number, typically in the range of Re=5,000 to 30,000. Wall damping function is needed to apply in the viscous-sublayer adjacent to the solid wall. For further details of this model, see Launder and Sharma (1974).

Fig. 4 shows the orthogonal grid systems generated with the help of the boundary integral technique (Kang and Leal 1992). For the single and double-hill models, the grid-size-independency was obtained with numerical grids of (110× 60) points and (130× 60) points, respectively (Kim *et al.* 1997).

Together with the standard $k-\varepsilon$ turbulence model, the following modified wall function (Tani 1987) was used to reflect surface roughness :

$$U = \frac{u_*}{\kappa}\ln\frac{z}{z_0} = \frac{u_*}{\kappa}\ln(Ez^+), \quad k = \frac{u_*^2}{\sqrt{C_\mu}}, \quad \varepsilon = \frac{u_*^3}{kz} \tag{7}$$

Here, z^+ is defined by $u_* z/\nu$ and C_μ is the model constant associated with the eddy viscosity. In the law of the wall, the constant E is defined as $E=\exp\{\kappa(B-\Delta B)\}$, B is given as 5.2 and ΔB varies with surface roughness (Kim *et al.* 1997). For high Reynolds number flows, numerical difficulty was encountered in locating several grids within the thin viscous sublayer. No-slip condition was imposed on the terrain surface.

The inlet boundary condition for the turbulence quantities k and ε was approximated as

$$k = (\overline{u'^2} + \overline{v'^2} + \overline{w'^2})/2 = 1.5\overline{u'^2}, \quad \varepsilon = k^{1.5}/C_i D \tag{8}$$

Here, u', v', w' are the fluctuating velocity components, C_i is empirical constant (=0.3) and D is the hydraulic diameter ($D=4A/P=0.6$ where A is the inlet area and P is its perimeter) of the test section. We used the mass flow boundary condition to specify the outlet boundary condition.

4. Results and Discussion

4.1. Flow visualization

Figs. 5(a),(b) show the flows around the single and double-hill models visualized using the smoke-wire method at the reduced free-stream velocity of $U_\infty = 2$ m/s. For the single hill model, the flow is accelerated along the windward side and separated from the hill crest. The recirculation zone starts near the hill crest and extends up to the reattachment point. On the other hand, for the double-hill model with gap distance of $G = L_1$, the reattachment point behind the second hill is located about $x/h = 2.5$ from the second hill top. In addition, the turbulent shear layer between two adjacent hills is deflected upwards. Fig. 6 shows the numerically simulated streamline contours around the single and double-hill models. The streamlines are roughly well matched with the streaklines shown in Fig. 5.

The oil-ink dot method (Langston and Boyle 1982) and tuft method were also employed to find the reattachment point of the separated shear flow behind the sinusoidal hill models. These flow visualization experiments were carried out at the free-stream velocity of $U_\infty = 10$ m/s. The reattachment points determined from this flow visualizations and the numerical prediction are compared in Table. 1. The numerical results overestimate the reattachment point about 20%, compared with the experimental results.

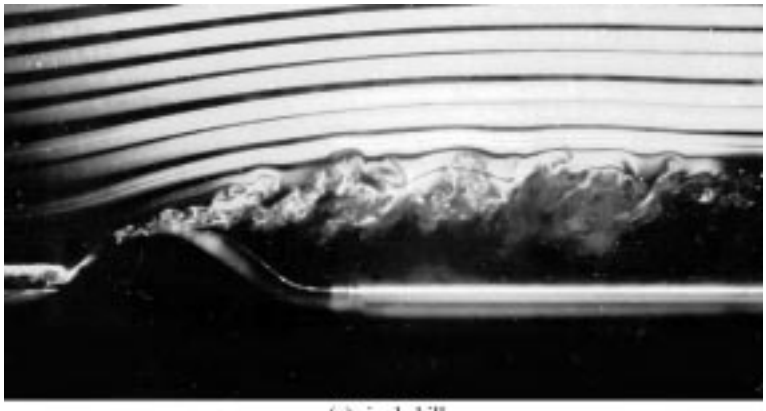

(a) single hill

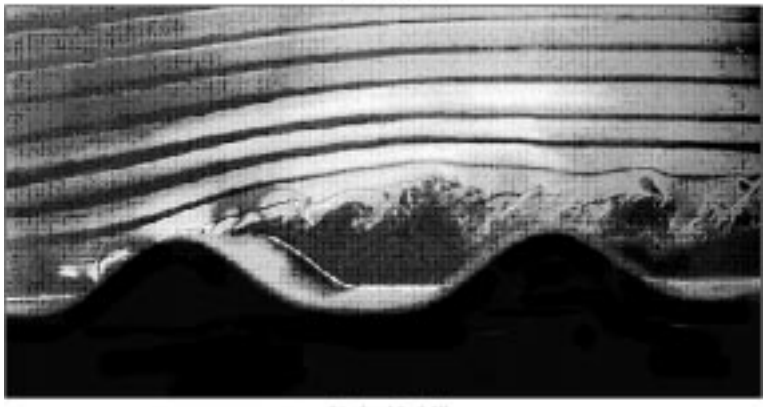

(b) double hill

Fig. 5 Visualized flow around single and double hills

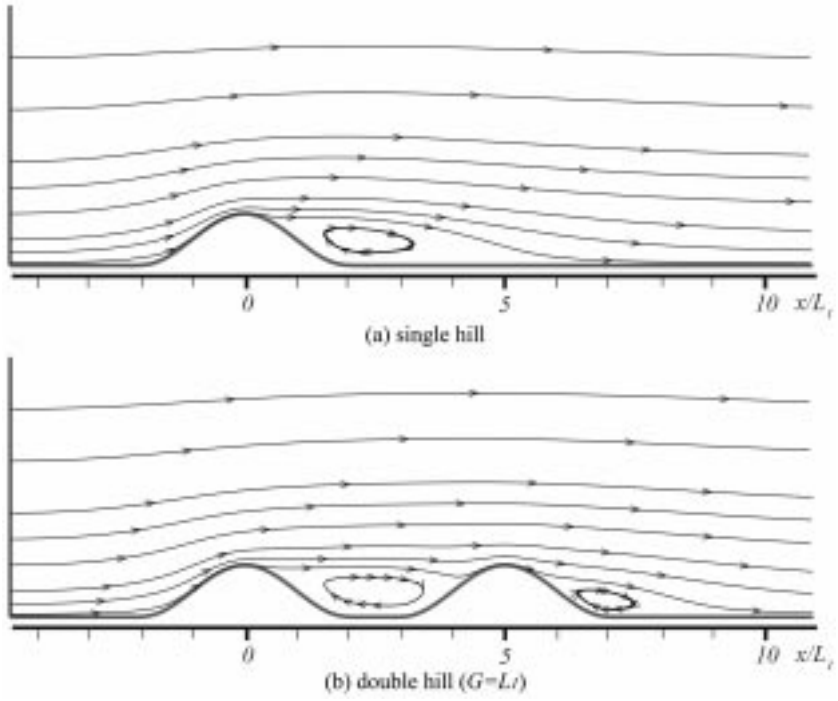

Fig. 6 Numerically simulated flow around single and double hills

Table 1 Comparison of reattachment points

	Reattachment Point(Experimental)	Reattachment Point(Numerical)
Single Hill	$4.25h \pm 0.25h$	$5.02h$
Double Hill	$2.5h \pm 0.25h$	$3.0h$

It should be noted that the momentum transfer over sinusoidal obstacles is considerably different from that of bluff obstacles. Petryk and Brundrett (1967) found that the recirculation zone formed behind a two-dimensional fence extends up to $x/h=17$. Therefore, the recirculation zones formed behind the sinusoidal hill models tested in this study are comparatively small.

4.2. Mean flow field

Fig. 7 shows the vertical profiles of mean streamwise velocity for the single hill. In this figure, the solid line behind the hill indicates the separated recirculation region predicted for the single hill with slope of 0.5. The on-coming flow forms a considerably thin boundary layer on the windward surface of the hill and is accelerated as it approaches to the hill crest. Compared with the previous results for the hilly terrain immersed in an atmospheric boundary layer, the speed-up on the hill top in a uniform flow is obviously prominent (Kim *et al*. 1997). Although there is a little discrepancy in the separated shear layer behind the hill, the overall comparison between the experimental results and numerical prediction show a good agreement.

Flow fields over a double-hill models were investigated with varying the gap distance between

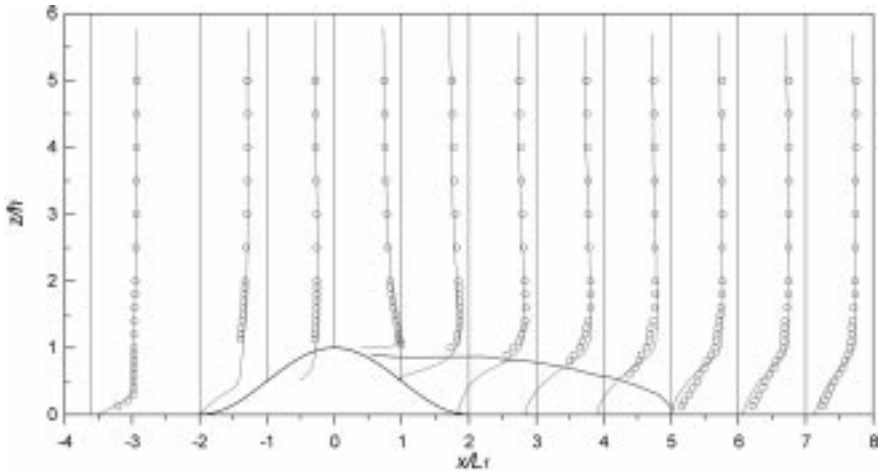

Fig. 7 Mean streamwise velocity profiles over a single hill (○ , measurement; – , numerical prediction)

two hills of same shape. Fig. 8 represents the mean streamwise velocity profiles around double-hills having different gap distance. The comparison between numerical prediction and experimental results also shows a reasonable agreement. Although the flow over the first hill shows similar flow pattern, the shear layer between two hills has different flow structure, especially the shape and size of the recirculation region formed between two hills are different. Except for the case of $G=6L_1$, the flow separated from the first hill forms a large recirculation region extended to the windward slope of the second hill. However, the shape and size of the separation bubbles formed behind the second hills are nearly similar, irrespective of the gap distance. They are about 30~40% smaller than that formed behind a single hill. This maybe results from the adverse pressure gradient between two hills and the momentum loss when the flow passes over hills.

4.3. Mean surface pressure distribution

The surface pressure distribution on a single hill is shown in Fig. 9. The pressure coefficient C_p decreases on the windward slope due to flow acceleration and has the minimum peak-value near the hill top where the maximum speed-up takes place. In the leeside of the hill, the momentum loss due to viscous and vorticity dissipation prevents the surface pressure to recover that of on-coming flow in the upstream of the hill. On the hill top ($x/L_1=0$), the numerical result is larger than the measured pressure coefficient. The discrepancy seems to be caused by the turbulence model that has some limitations in estimating this kind of highly turbulent shear flows. Compared with the surface pressure measured for the same hill model immersed in an atmospheric boundary layer. (Kim *et al*. 1997) The surface pressures on the sinusoidal hill immersed in a uniform flow have much smaller values due to relatively high-speed of on-coming flow near the ground surface as shown in Fig. 5.

The surface pressure distributions for the double-hill models are shown in Figs. 10(a)~(d). Similar to the case of single hill, the calculated pressure coefficients predict well the experimental results except the region near the hill top. It should be mentioned that the local minimum C_p at the second hill crest is about 25~30% smaller than that at the first hill crest. In addition, the minimum C_p at the first hill top is nearly unchanged. However, the local minimum C_p at the second hill top is decreased as the gap distance increases. From this, we can see that the approaching flow loses nearly the same

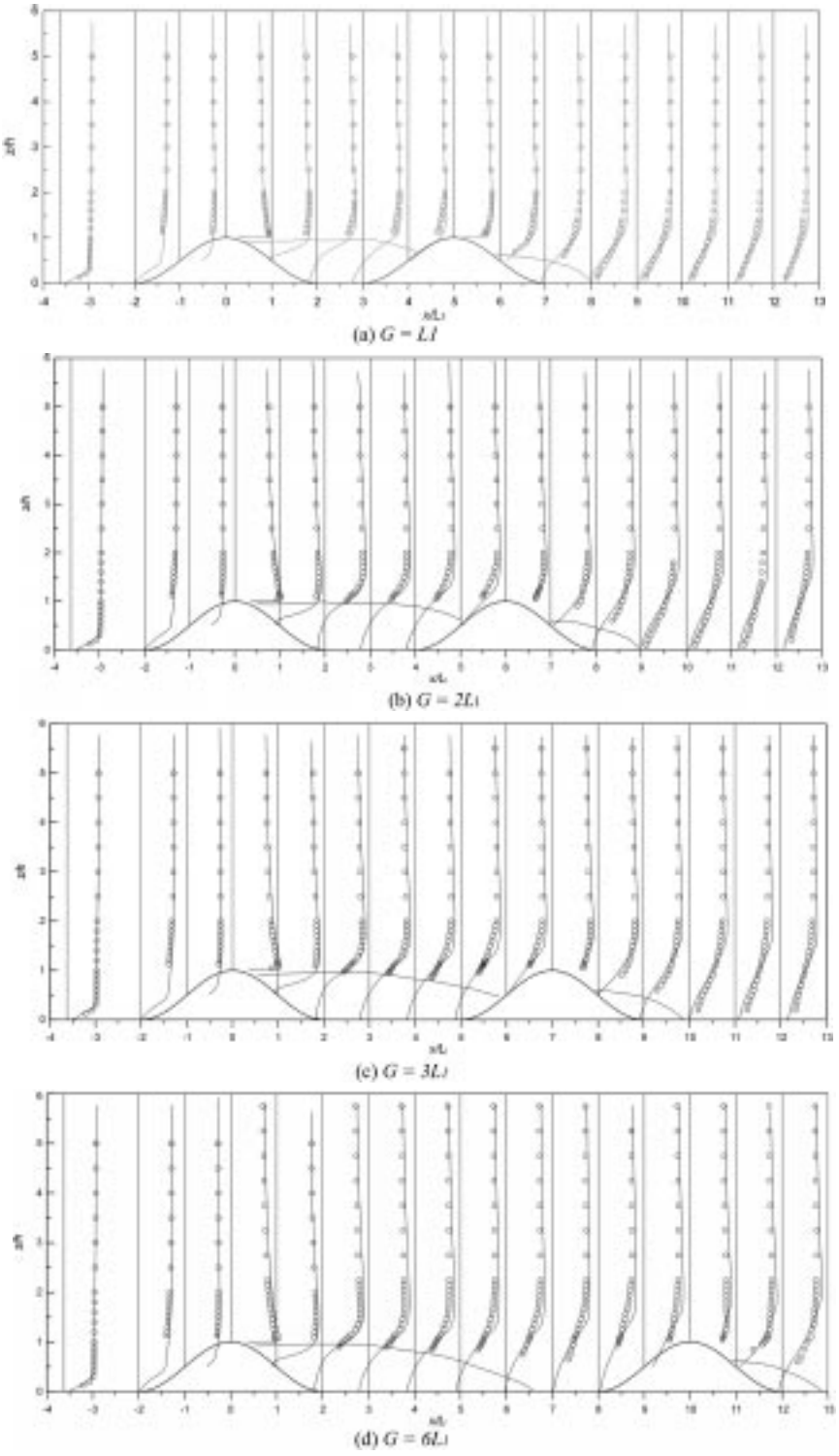

Fig. 8 Vertical profiles of mean streamline velocity over double-hills

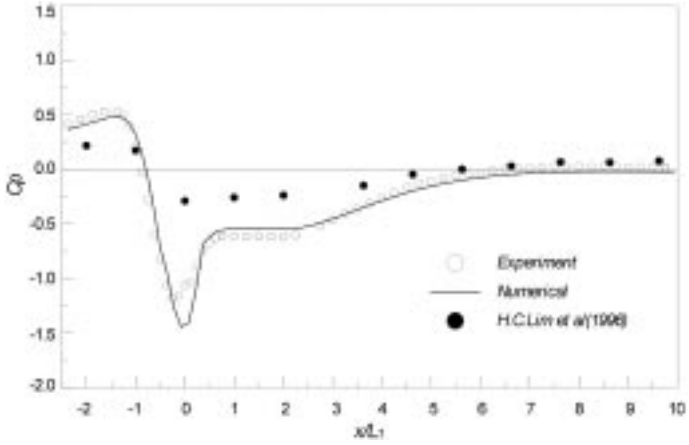

Fig. 9 Surface pressure distribution over a single hill

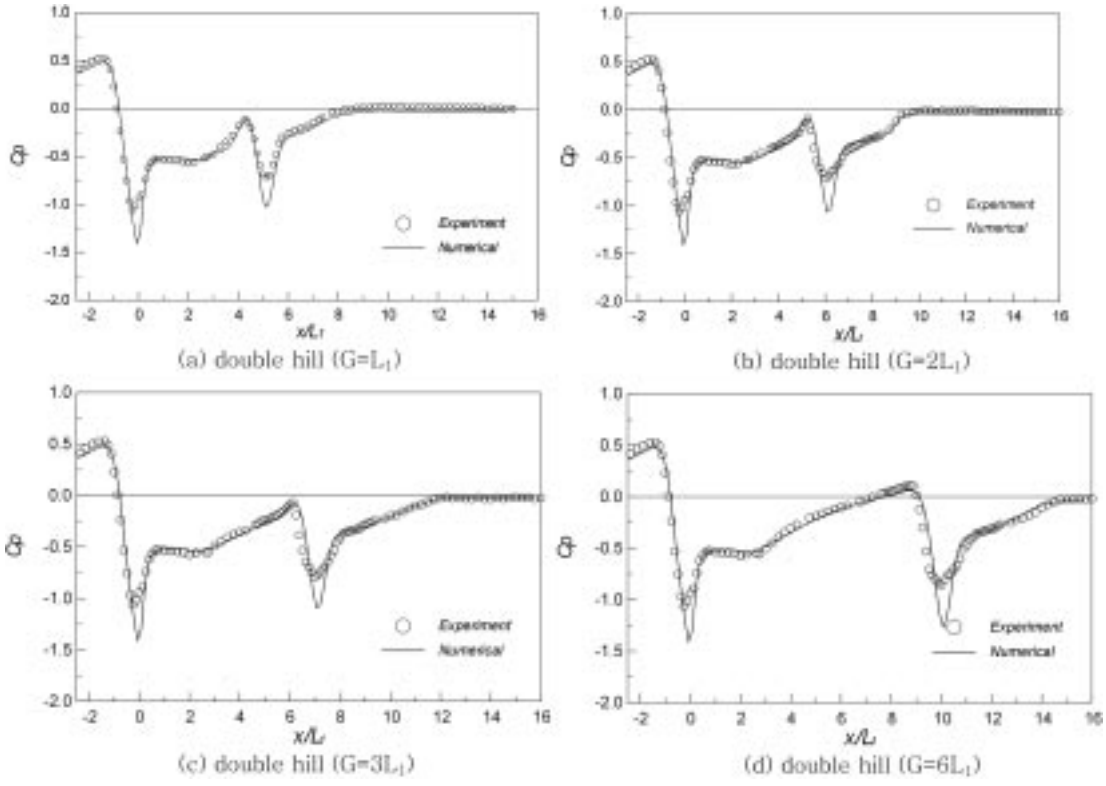

Fig. 10 Surface pressure distributions over double-hills

amount of momentum when it passes over the first hill, however, the shear flow separated from the first hill disturbs the flow over the second hill in a different extent depending on the gap distance. In Fig. 10(d), the surface pressure exceeds its static pressure at the front foot of the second hill. This results from the reattachment of the separated shear layer in front of the second hill as shown in Fig. 8(d).

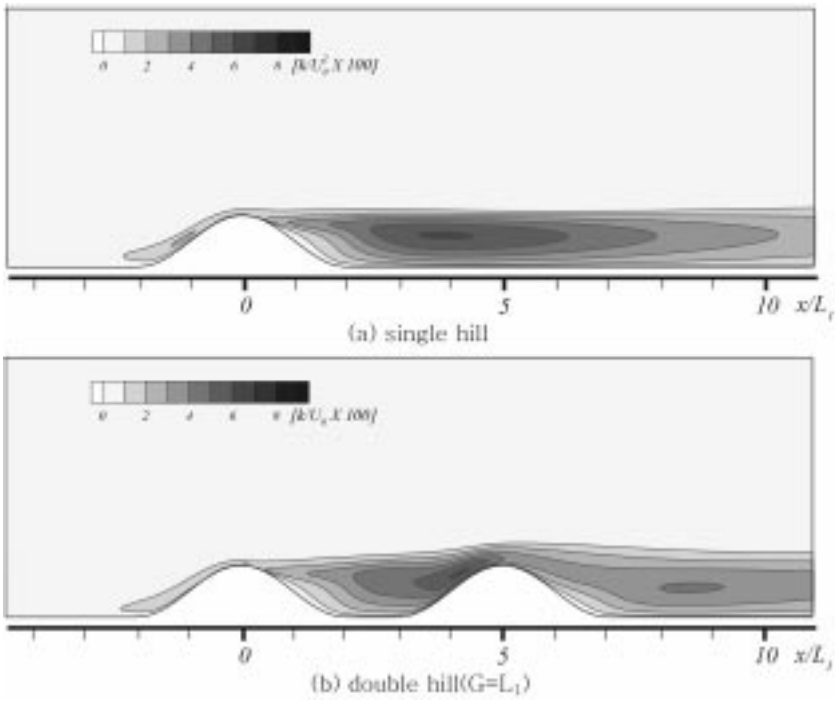

Fig. 11 Turbulent kinetic energy over a single hill and double hill

4.4. Turbulent statistics

Fig. 11 shows the contour plots of turbulent kinetic energy of flow over the single and double-hill models. The hilly terrain disturbs the on-coming flow and the effect of the perturbed flow can be found in the spatial distribution of turbulent kinetic energy. Bradshaw (1973) mentioned that the turbulent kinetic energy is increased due to flow separation in the leeside of the hill. On the other hand, the mild velocity gradient in the upstream of the hill does not increase the turbulent kinetic energy enough to recognize. For a single hill, the turbulent kinetic energy has its maximum value at the location of about $x/L_1=4$ and $z/h=0.6$ in the separated shear layer behind the hill. Thereafter it is decreased slowly by viscous dissipation.

However, for the double-hill model, the shear layer separated from the first hill hits on the windward slope of the second hill. Therefore, the turbulent kinetic energy has the maximum value at the upstream hillside of the second hill. The turbulent kinetic energy of flow passing over the second hill is recovered slowly with going downstream.

5. Conclusions

The wind flow over two-dimensional sinusoidal hilly obstacles with slope of 0.5 has been investigated experimentally and numerically. Mean velocity profiles, turbulent kinetic energy, and surface pressure distributions were measured for single and double-hill models. The numerical simulation based on the finite-volume-method and the SIMPLE-C algorithm with an orthogonal body fitted grid system is employed. The results are summarized as follows :

1. The mean velocity profiles and surface pressure distributions measured in the wind tunnel experiments are in a good agreement with the numerical predictions except the hill top region. In the region near the hill crest, the numerical results underestimate the surface pressures measured in the wind tunnel tests.
2. For hilly obstacles immersed in a uniform flow, the surface pressure coefficient near the hill crest is smaller than that in an atmospheric boundary layer due to relatively high-speed flow near the hilly terrains.
3. For the double-hill models having gap distances smaller than $G = 6L_1$, the flow separated from the first hill forms a large recirculation region extended to the second hill. The separation bubbles formed behind the second hill are nearly unchanged, irrespective of the gap distance. They are about 30~40% smaller than that behind a single hill.
4. For the double hill models, the surface pressures on the first hill crest are nearly unchanged. However, the surface pressures on the second hill crest are about 25~30% smaller than those at the first hill top and the difference is decreased as the gap distance increases.

Acknowledgement

This work was supported by NRL(National Research Laboratory) project and POSTECH.

References

Bergeles, G. (1985), "Numerical calculation of turbulent flow around two-dimensional hills", *J. Wind Eng. Ind. Aerody.*, **21**, 307-321.

Bowen, A.J. and Lindley, D. (1977), "A wind tunnel investigation of the wind speed and turbulence characteristics close to the ground over various escarpment shapes", *Boundary-Layer Meteorol.*, **12**, 259-271.

Bradshaw, P. (1973), "Effects of streamline curvature on turbulent flow", *Agardograph*, 169.

Glekas, J., Bergeles, G. and Athanassiadis N. (1987), "Numerical solution of the transport equation for passive contaminations in three-dimensional complex terrain", *Int. J. Num. Meth. Fluids*, **7**, 319-335.

Jackson, P.S. and Hunt, J.C.R. (1975), "Turbulent flow over a low hill", *Quart. J. Roy. Meteorol. Soc.*, **101**, 929-955.

Jones, W.P. and Launder, B.E. (1972), "The prediction of laminarization with a two-equation model of turbulence", *Int. J. Heat Mass Transfer*, **15**, 301-314.

Kang, I.S. and Leal, L.G. (1992), "Orthogonal grid generation in a 2D domain via the boundary integral technique", *J. Comput. Phys.*, **102**, 78-87.

Kim, H.G., Lee, C.M., Lim, H.C., and Kyong, N.H. (1997), "An experimental and numerical study on the flow over two-dimensional hills", *J. Wind Eng. Ind. Aerod.*, **66**, 17-33.

Langston, L.S. and Boyle, M.T. (1982), "A new surface-streamline flow-visualization technique", *J. Fluid Mech.*, **125**, 53-57.

Launder, B.E. and Sharma, B.T. (1974), "Application of the energy dissipation model of turbulence to the calculation of flow near a spinning disc", *Lett. Heat Mass Transfer*, **1**, 131-138.

Pearse, J.R. (1982), "Wind flow over conical hills in a simulated atmospheric boundary layer", *J. Wind Eng. Ind. Aerod.*, **10**, 303-313.

Petryk, S. and Brundertt, E. (1967), Department of Mechanical Engineering, Univ. of Waterloo, Res. Rep. No. 4.

Siegel, R. (1976), "Three-dimensional potential flow over hills and oval mounds", NASA Tech. Note TN D-8375.

Tani, I. (1987), "Turbulent boundary layer development over rough surface", *Perspectives in Turbulence Studies*, Meier, H. U. and Bradshaw, P., Eds., Springer.

Taylor, P.A. (1997), "Turbulent boundary-layer flow over topography", *2nd European & African Conference on Wind Engineering*, 25-44.

Wilcox, D.C. (1993), "Turbulence modeling for CFD", DCW Industries, Inc., 460.

CC